Microsc. Microanal. 12, 26–35, 2006
DOI: 10.1017/S143192760606020X

Microscopy AND Microanalysis

The New X-ray Mapping: X-ray Spectrum Imaging above 100 kHz Output Count Rate with the Silicon Drift Detector

Dale E. Newbury*

Surface and Microanalysis Science Division, National Institute of Standards and Technology, Gaithersburg, MD 20899-8370, USA

Abstract: Electron-excited X-ray mapping is a key operational mode of the scanning electron microscope (SEM) equipped with energy dispersive X-ray spectrometry (EDS). The popularity of X-ray mapping persists despite the significant time penalty due to the relatively low output count rates, typically less than 25 kHz, that can be processed with the conventional EDS. The silicon drift detector (SDD) uses the same measurement physics, but modifications to the detector structure permit operation at a factor of 5–10 times higher than conventional EDS for the same resolution. Output count rates as high as 500 kHz can be achieved with 217 eV energy resolution (at MnKα). Such extraordinarily high count rates make possible X-ray mapping through the method of X-ray spectrum imaging, in which a complete spectrum is captured at each pixel of the scan. Useful compositional data can be captured in less than 200 s with a pixel density of 160×120. Applications to alloy and rock microstructures, ultrapure materials with rare inclusions, and aggregate particles with complex chemistry illustrate new approaches to characterization made practical by high-speed X-ray mapping with the SDD.

Key words: electron beam microanalysis, energy dispersive X-ray spectrometry, microstructural characterization, particle analysis, scanning electron microscopy, silicon drift detector

Introduction

In the 50 years since the technique of elemental mapping by electron-beam-excited X-ray emission was developed by Cosslett and Duncumb (1956), "X-ray mapping," as it has become known, has proven to be one of the most popular operational modes of electron probe microanalysis (EPMA) for the characterization of complex microstructures (Goldstein et al., 2003). X-ray mapping produces images of elemental distributions with micrometer lateral and depth spatial resolution (and occasionally submicrometer resolution) that provide a visually powerful data presentation. With X-ray maps, the analyst can readily recognize specific local chemical variations that may not be visible, or at least readily interpretable, in associated scanning electron microscope (SEM) "compositional contrast" images, for instance, atomic number contrast from backscattered electrons. Early X-ray mapping was performed with either energy dispersive spectrometry from a gas proportional counter, which suffered from very poor energy resolution that limited detectability, or with the high-resolution wavelength dispersive spectrometer (WDS), which had high count rate capability and high spectral resolution but which was restricted to measuring a single element per area scan. For mapping multiple elements in the same area, the WDS had to be retuned to another elemental peak and the scan repeated. Mapping elements in parallel required multiple WDS. The efficiency of elemental mapping was significantly increased by the introduction of the silicon (lithium-compensated) energy dispersive X-ray spectrometer (Si(Li)-EDS) (Fitzgerald et al., 1968), which had much improved energy resolution compared to the flow proportional counter. Si(Li)-EDS enabled elements throughout the entire range of electron-excited X-ray energies to be measured simultaneously through the use of electronic signal processing. Rapid advances in laboratory computing power, speed, and data storage led to the development of X-ray spectrum imaging (XSI) (Gorlen et al., 1984), in which the entire EDS spectrum was recorded at each beam location (pixel). XSI achieves the ultimate in compositional information capture: In principle, unexpected elemental features can be detected in an

Received September 26, 2005; accepted October 18, 2005.

Note: The Siegbahn notation for characteristic X-rays is commonly used in the field of electron beam X-ray spectrometry and will be used in this article. The equivalent IUPAC notation is indicated in parentheses at the first use.

In this article, the following arbitrary definitions will be used when referring to concentration (C) ranges: major: $C > 0.1$ (10 wt%), minor: $0.01 \leq C \leq 0.1$ (1–10 wt%), and trace: $C < 0.01$ (1 wt%).

*E-mail: Dale.Newbury@nist.gov

X-ray spectrum image because all possible spectrum information, within the performance limits of the Si(Li) EDS, is captured at each pixel.

X-ray mapping has achieved this high degree of popularity despite the considerable penalty in instrument time that must be accepted to obtain statistically robust X-ray mapping data, especially with Si(Li)-EDS. Unfortunately the maximum output count rate with the Si(Li)-EDS when operating under "best resolution" conditions (i.e., long peaking time constant) is limited to approximately 2,000 counts per second (cps). Useful spectral measurements for "point" analysis (i.e., fixed beam position) typically require 10 s or more to obtain robust statistics adequate for measurement and quantification of major constituents. Detection of minor and trace constituents requires even longer accumulation time. When X-ray mapping is performed, the beam must be scanned over an array of points, for example, 128 × 128, which has the inevitable effect of limiting the dwell time at each pixel. Even if the pixel dwell is reduced by a factor of 100 (relative to point analysis conditions) to 100 ms, so that only major constituents could likely be measured at a single pixel in the map, the total time (live time) needed for a map would be 1638 s. Achieving adequate X-ray counts to capture at least part of the minor constituent range with single pixel sensitivity (1 s dwell) would require 16,384 s (4.6 h) or even longer.

The emergence of a new class of energy dispersive X-ray spectrometer, the silicon drift detector (SDD) (Struder et al., 1998; Barkan et al., 2004; Newbury, 2005), promises to radically change the measurement situation for energy dispersive X-ray spectrometry, especially with regard to X-ray mapping. For a given detector active area, an SDD can achieve slightly better energy resolution than the conventional Si-EDS, for example, an SDD of a 50-mm^2 area can operate at a resolution of 134 eV (at MnKα; IUPAC: K-L$_{2,3}$), measured as the full peak width at half maximum intensity (FWHM) versus approximately 140 eV for a conventional 50 mm^2 Si(Li)-EDS. The SDD can operate with modest cooling, −20°C to −60°C, which can be achieved with Peltier cooling, compared to the Si(Li)-EDS, which is typically cooled with liquid nitrogen to −190°C. However, the greatest advantage of the SDD as an analytical tool is that for a given resolution, the SDD can provide a much higher count output count rate (OCR) versus input count rate (ICR), as shown in Figure 1 and Table 1 from experimental measurements performed with a 50 mm^2 SDD (Newbury, 2005). At 134 eV resolution (8 μs peaking time) this SDD achieved a maximum OCR of 14,000 cps. By comparison, the maximum output count rate for a conventional 30-mm^2 Si-EDS operating under "best resolution" conditions (134 eV at MnKα with a peaking time of 50 μs) was 1800 cps, whereas the choice of a peaking time of 4 μs extended the maximum output count rate to approximately 30,000 cps with a resolution of 178 eV. The SDD can achieve a maximum OCR of 160,000 cps with a resolution of 163 eV. In addition, it is possible to design an SDD that demonstrates extremely good peak integrity with counting rate, as shown in Figure 2 for the peak resolution and in Figure 3 for the peak channel position. Peak integrity with count rate is a feature that is important for X-ray mapping because even at constant electron beam current, the local composition will have a strong effect on the rate of X-ray production, so that as the beam is scanned, the input count rate may vary by a factor of 10 or more from location to location in a single map.

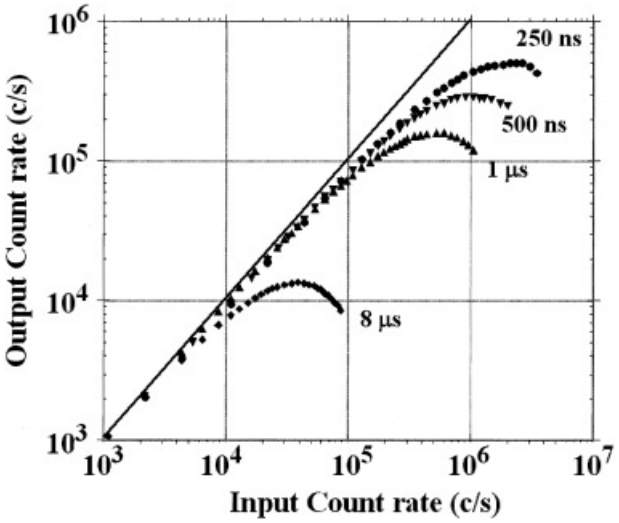

Figure 1. Output count rate versus input count rate for four different time constants for a third-generation SDD. The points denote actual experimental measurements. The solid line represents the "ideal" response in the absence of deadtime (Newbury, 2005).

Experimental

Silicon Drift Detector

For this work, X-ray spectrum image mapping was performed with a Radiant Detectors LLC (Northridge, CA, USA) "Vortex" SDD of 50 mm^2 active area mounted on a Japan Electron Optics JEOL-840 scanning electron microscope equipped with a conventional tungsten filament gun.

Table 1. SDD Performance (Radiant Detectors LLC 50 mm^2 Vortex SDD)

Peaking time	Resolution (MnKα)	Maximum output count rate
8 μs	134 eV	14,000 cps
1 μs	163 eV	160,000 cps
500 ns	188 eV	280,000 cps
250 ns	217 eV	500,000 cps

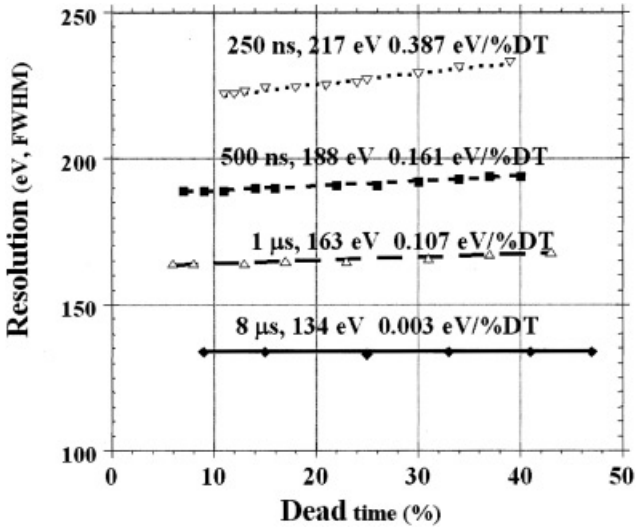

Figure 2. Peak resolution (full width, half maximum) as a function of input count rate, expressed as the percent dead time. The slope of each curve (electron volts per percent dead time) is indicated (Newbury, 2005).

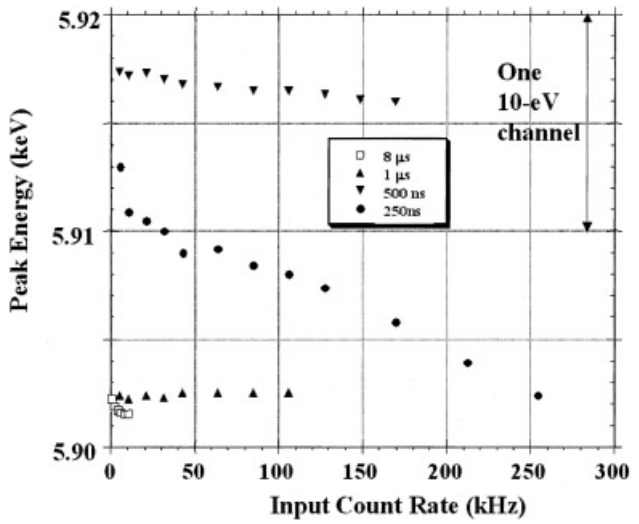

Figure 3. Peak energy (MnKα) versus input count rate at various peaking times: 8 μs, 1 μs, 500 ns, and 250 ns.

The SDD was controlled by Radiant Detectors LLC software and the output from the digital signal processor (DSP) incorporated in the Vortex system was processed through one of two software systems: "SAMx" (Levens, France) for the earlier work and more recently the 4pi Analysis "Revolution" (Durham, NC, USA).

Measurement Conditions

X-ray spectrum images (XSI) were recorded with the following parameters: 128 × 128, 160 × 120, or 80 × 60 pixels; 2048 channels (10 eV width); 2-byte intensity depth (65,536 counts maximum per channel). The pixel dwell time was chosen according to the nature of the experiment. The time overhead necessary to scan the beam and record the pixel spectrum was 1.3 ms for the SAMx software and approximately 0.5 ms for the 4pi Revolution software.

The beam energy was 20 keV for all measurements, and the beam current was chosen to generate an adequate X-ray flux to reach the desired output count rate on a pure copper target as a chosen reference standard. The beam current was measured with an in-column Faraday cup and a digital picoammeter. Due to difficulties in calibrating this in-column Faraday cup with a known current source, the absolute value of the beam current was not known, but the repeatability was estimated to be better than 0.2% relative based on the independent measurement by the spectrometer of the integrated X-ray count from the Cu standard.

Table 2. Composition of Phases in Raney Nickel (Analysis by NIST-NIH DTSA ZAF with pure element standards)

	Mass fraction ($\sigma_{\text{Concentration}}$, %)		
Phase	Al	Ni	Fe
Trace Ni	0.995 (0.2%)	0.005 (5.2%)	0
Low Ni (Fe)	0.712 (0.13%)	0.246 (0.4%)	0.042 (0.8%)
Intermediate Ni	0.600 (0.17%)	0.400 (0.3%)	0
High Ni	0.465 (0.22%)	0.535 (0.2%)	0

Test Specimens

Raney nickel, a methanation catalyst alloy (as-received bulk alloy, not chemically leached), was chosen as a test specimen because the composition, listed in Table 2, provides three phases with widely varying composition in the major constituents (aluminum and nickel) of the alloy as well as a localization of a minor constituent (iron) into a fourth distinct phase (source: U.S. Bureau of Mines, Pittsburgh, PA). Moreover, the characteristic X-ray peak for Al (AlKα = 1.487 keV) occurs in the low photon energy range (generally considered to be below 3 keV) whereas Ni provides characteristic peaks in the high photon energy range (NiKα = 7.47 keV and NiKβ [IUPAC: K-$M_{4,5}$] = 8.27 keV) as well as the low photon energy range (NiLα [IUPAC: L_3-$M_{4,5}$] = 0.849 keV).

Ferrovac, a high purity iron, was chosen as a test specimen because of its low level of impurities that nevertheless form rare, localized inclusions (source: Dr. Richard Ricker, NIST). The nominal composition of this material based upon bulk analysis for the batch by the manufacturer included oxygen at a concentration of 0.00091 (atom fraction) and silicon at 0.00016 (atom fraction).

Tetrahedrite, a copper–antimony sulfide in a calcite matrix from Peru, features a complex microstructure with

minor phases at low abundance (source: Department of Mineral Sciences, Smithsonian Institute, Washington, DC).

Polished cross sections of the Raney nickel, Ferrovac iron, and tetrahedrite were prepared by conventional metallographic preparation techniques followed by carbon coating to minimize charging effects.

Particles of slag from a coal-fired power plant (Chalk Point, MD) collected during a study of particulate emissions (Small, 1976) were dispersed on an adhesive carbon tape substrate and carbon coated. These particles often have heterogeneous compositional structures.

X-ray Spectrum Image Interpretation

XSI databases were interpreted using National Institutes of Standards and Technology LISPIX, a comprehensive image processing software engine (Bright, 1995, 2003). LISPIX has recently been augmented with "derived spectrum" software tools specifically designed for interpreting spectrum images (Newbury & Bright, 2005). The SUM spectrum is determined by adding the counts at all pixels in each channel image to create the derived spectrum of X-ray intensity plotted versus channel number (i.e., X-ray energy). Elements that occur with high abundance in the XSI appear as prominent peaks in the SUM spectrum. The MAXIMUM PIXEL spectrum is created by determining the maximum X-ray count at any pixel within each channel image and plotting that maximum versus channel number. The RUNNING MAXIMUM is calculated by first averaging the X-ray count data over several energy channels, for instance, the channel of interest and two channels above and below, followed by the application of the MAXIMUM PIXEL operation to the smoothed data. Both the MAXIMUM PIXEL and the RUNNING MAXIMUM derived spectrum tools provide great sensitivity to rare features in the XSI, with sensitivity demonstrated to extend to single-pixel compositional features (Newbury & Bright, 2005). Thus, a typical analysis sequence consisted of applying the SUM derived spectrum tool to determine the dominant features in the XSI, followed by the MAXIMUM PIXEL and RUNNING MAXIMUM tools to detect rare features. After a peak of interest was identified in the derived spectrum, LISPIX was used to construct the *x*-*y* image that corresponded to that peak channel or range of contiguous channels that spanned the peak.

Results

X-ray Spectrum Image Mapping in Short Time Intervals

The extraordinary output count rates obtainable with the SDD, shown in Figure 1, make the X-ray spectrum imaging method extremely attractive for elemental mapping. Comprehensive X-ray spectrum image mapping becomes possible in time periods of only a few minutes. To demonstrate the minimum time limits for SDD XSI containing useful compositional information, Raney nickel was mapped with the SDD operating with a peaking time of 250 ns, which provides a resolution of 217 eV (at MnKα). A sufficient beam current was selected to provide an output count rate (measured while overscanning the full field to be mapped) of approximately 250 kHz. From the OCR versus ICR behavior shown in Figure 1 for the 250-ns peaking time, this choice would appear to be well below the peak OCR of 500 kHz and unnecessarily conservative. However, in X-ray mapping, careful attention must be given when selecting the incident beam current as to the actual range of output count rate as different phases are sampled within the scanned area of the map. In the case of Raney nickel, the aluminum-rich phase, which is nearly pure aluminum (0.995 mass fraction) with only 0.005 nickel produces a substantially higher output count rate, by a factor of about 2, for a given beam current than the other phases that contain higher nickel (and for one phase, iron) contents. The overvoltage at $E_0 = 20$ keV for the Al *K*-shell is much higher ($U_{Al} = 13.4$) compared to the Ni *K*-shell ($U_{Ni} = 2.4$), generating a higher X-ray production rate for AlKα radiation, which dominates the OCR behavior despite the losses due to greater self-absorption of the AlKα radiation compared to NiKα.

Each X-ray spectrum image was collected with a pixel scan of 160 × 120, and various dwell times were used, as listed in Table 3. The clock time included the dead time correction as well as the pixel overhead involved with beam control and spectrum storage. The resulting X-ray spectrum image databases were examined with NIST LISPIX, and the SUM spectrum was used to extract the X-ray intensity maps that corresponded to the major peaks from aluminum and nickel, the principal constituents of the Raney nickel alloy. The elemental X-ray images were derived for the characteristic peaks with appropriate windows necessary to span the peaks: AlKα, 150-eV-wide window; FeKα, 200-eV-wide window; NiKα, 200-eV-wide window. These elemental maps, shown in Figure 4, provide virtually the

Table 3. SDD Mapping Conditions for Raney Nickel, 160 × 120 Pixels; Dead Time ~ 25%

Pixel dwell	Live seconds	Clock seconds
50 ms	960	1210
10 ms	192	250
5 ms	96	130
2 ms	38	58
1 ms	19	34

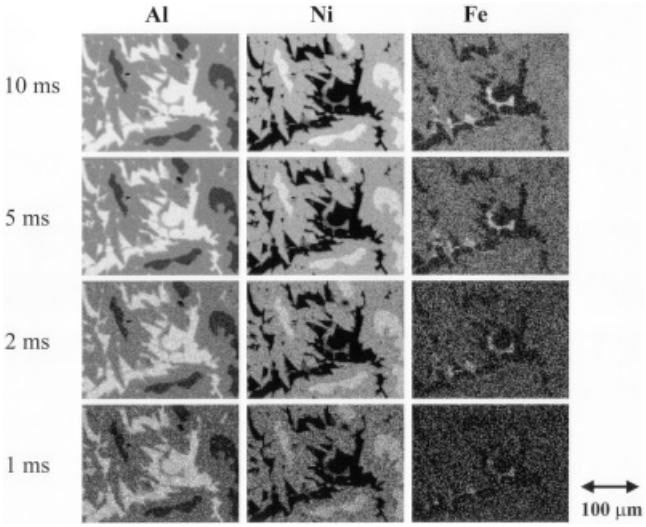

Figure 4. Elemental X-ray images derived for characteristic peaks (AlKα, 150-eV-wide window; FeKα, 200-eV-wide window; NiKα, 200-eV-wide window) from X-ray spectrum images recorded with various pixel dwell times: 10 ms, 5 ms, 2 ms, 1 ms.

same overall information about the region being imaged, even with a pixel dwell time of only 1 ms. For the output count rate achieved, a 1-ms dwell provides only about 200 counts in the entire spectrum at the average pixel. Perhaps more surprising is the persistence of the visibility of the minor iron component, also shown in Figure 4, as the pixel dwell time is reduced. The iron constituent is readily visible with a 2-ms pixel dwell, and some iron-containing regions are still visible with only 1 ms dwell, although it is questionable if those iron-rich regions would be recognizable without the prior knowledge given by the longer dwell maps. Note that the images for FeKα in Figure 4 have not been corrected for background. The apparent low level segregation of iron to the nickel-rich phases, as compared to the aluminum-rich phase, is an artifact of the atomic-number dependence of the X-ray continuum.

Applying X-ray Mapping Where It Was Previously Impractical

Although X-ray mapping has solved many important problems in its 50-year history, there are certain classes of problems for which mapping with the conventional EDS has been impractical because of the need to sample large areas of the specimen with multiple mapping runs, which results in exorbitant time demands. An example is the detection of rare inclusions in ultrahigh-purity materials. Through advanced methods of refining, the bulk impurity levels in such materials have been reduced to parts per million or even lower, resulting in interesting improvements in materials properties, especially corrosion resistance. A topic of interest in this field involves understanding the fate of the remaining impurities: Are these impurity atoms distributed homogeneously through the material or are there inclusions where the trace constituents collect locally? This characterization problem with X-ray mapping is fundamentally one of sampling. Because of the expected rarity of the inclusions, if they exist at all, many areas must be sampled. The conventional approach to this problem is to employ backscattered electron imaging (BSE), which gives a compositionally sensitive but nonspecific atomic number contrast. Although SEM-BSE imaging will always be a valuable tool because of its speed, there exist limitations on its application when features and matrix have a similar average atomic number, leading to an inevitable decrease in contrast.

Figure 5 shows an example of XSI mapping applied to the study of trace constituents in Ferrovac high-purity iron. The bulk trace analysis of this material reported oxygen at a concentration of 0.00091 (atom fraction) and silicon at 0.00016 (atom fraction). The field of interest, shown in Figure 5, was selected from many blank fields and contains several inclusions. These inclusions appear prominently in the SEM images of Figure 5a (Everhart-Thornley detector, positively biased to collect secondary and backscattered electrons) and Figure 5b (backscattered electron detector, sum mode). The MAXIMUM PIXEL SPECTRUM, as shown in Figure 5c, shows prominent peaks for iron, carbon, and oxygen, and a minor peak for silicon. The corresponding maps derived from the X-ray peaks for iron (Fig. 5f) and oxygen (Fig. 5d) reveal the compositional identity of the inclusions as oxides. When the minor silicon peak in the MAXIMUM PIXEL SPECTRUM is chosen and the corresponding silicon map is constructed (Fig. 5e), the trace silicon is found to be associated closely with the iron oxide inclusions. The color overlay (Fig. 5g) reveals that the trace silicon component forms on the boundaries of the iron oxide particles, probably as silicon oxide, and, in one case, it appears at the center of an iron oxide particle, perhaps acting as a nucleation site. Close inspection of the SEM images indicates that these Si-rich features are very difficult to discern, and they are likely to be missed with a search strategy based exclusively on SEM images, whereas XSI and derived spectrum software tools can readily locate these rare features.

Visualizing Compositional Contrast

A useful XSI can be collected in only a few minutes when a high beam current is used to create a high X-ray flux and the SDD is employed to measure the spectrum at each pixel in a map. The compositional contrast that can be derived from such an XSI with high X-ray counts compares favorably to the type of image information that we normally associate with SEM BSE imaging. An example of the contrast depth that can be achieved is shown in Figure 6, which

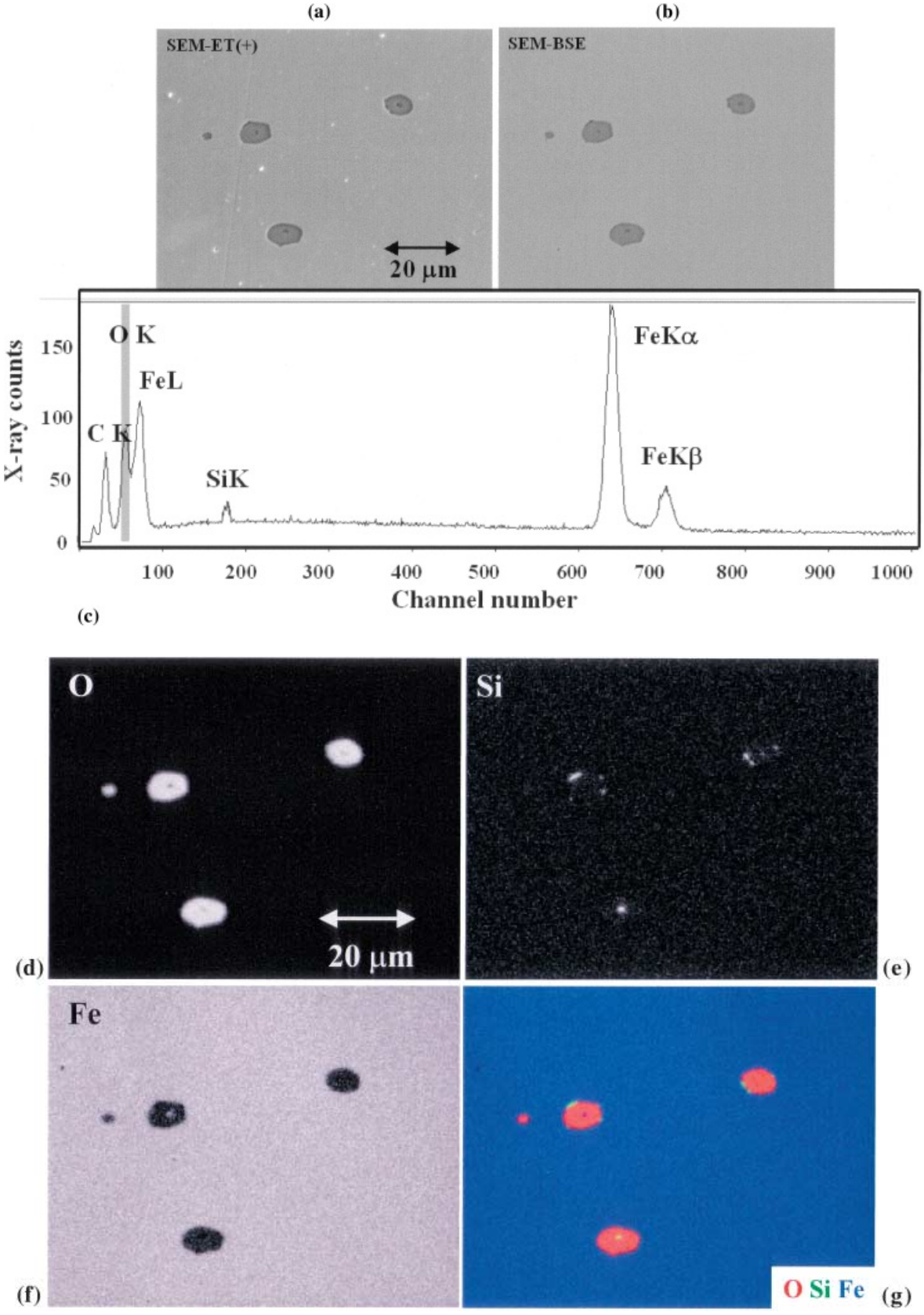

Figure 5. SEM images and X-ray maps derived from an X-ray spectrum image of Ferrovac high purity iron. **a**: SEM-Everhart Thornley detector, positively-biased. **b**: SEM backscattered electron image. **c**: MAXIMUM PIXEL derived spectrum. **d**: O K image. **e**: SiKα image. **f**: FeKα image. **g**: Color overlay: O = red; Si = green; Fe = blue.

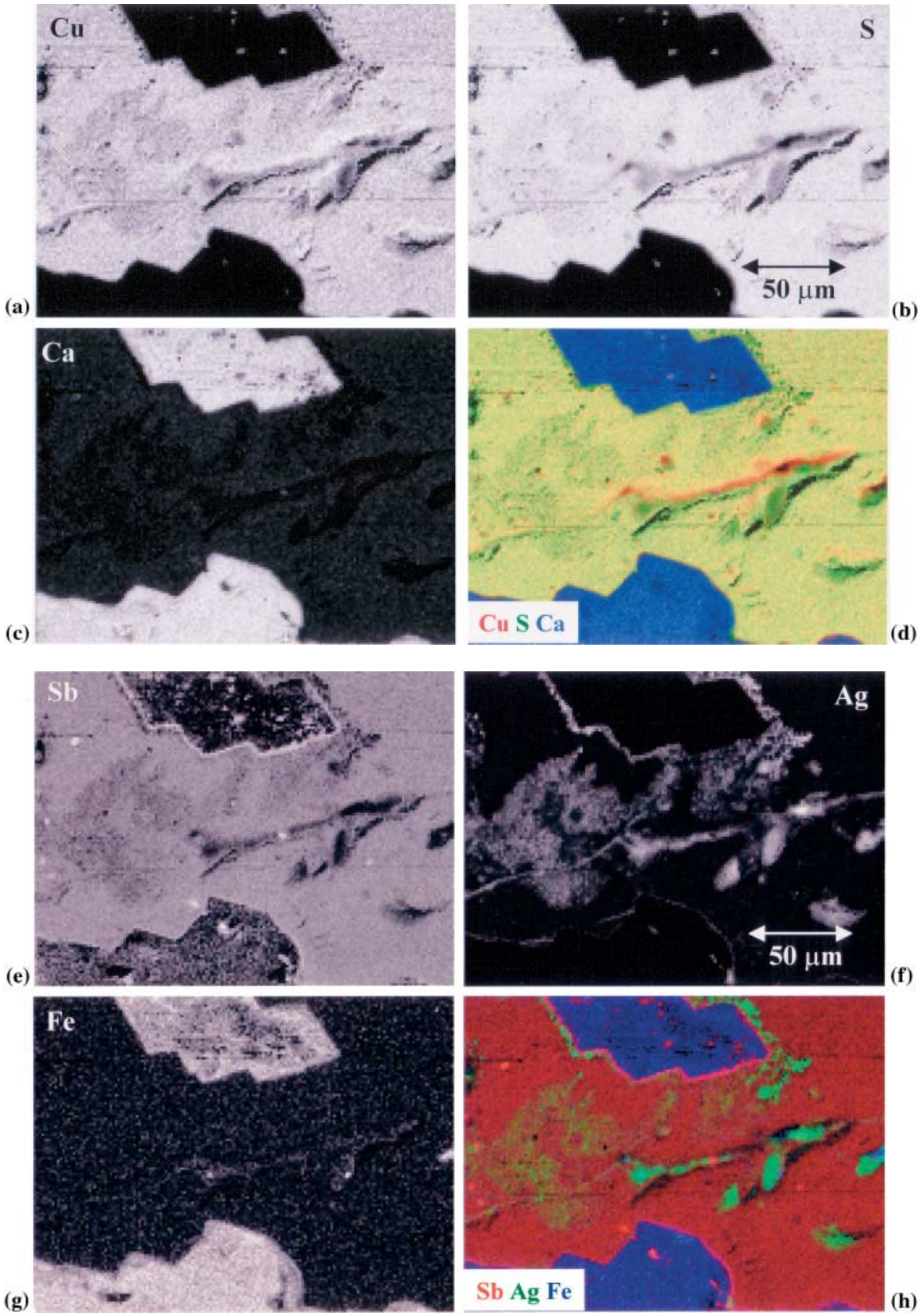

Figure 6. X-ray maps derived from a 12-min 160 × 120 pixel X-ray spectrum image of tetrahedrite (Peru). Major constituents: CuKα (**a**), S Ka (**b**), CaKα (**c**), color overlay with Cu = red, S = green, Ca = blue (**d**). Minor constituents: SbLα (**e**), AgLα (**f**), FeKα (**g**), color overlay with Sb = red, Ag = green, Fe = blue (**h**).

depicts the various elements in a rock microstructure consisting of a sulfide in a matrix of calcite as recovered from a 160 × 120 pixel XSI recorded in 12 min (50 ms per pixel). The X-ray maps for the major constituents, for example, Cu, S, and Ca, show fine-scale compositional structures that can only be discerned because of the locally high X-ray counts. Even the minor constituents, such as antimony, silver, and iron, were recorded with sufficient counts in this short time to discern fine scale compositional features. The contrast in the X-ray maps derived from the XSI rival what we are accustomed to seeing in BSE compositional images, but the X-ray maps are, of course, specific to the element in question.

Advanced Particle Analysis by XSI Mapping

Quantitative analysis of microscopic particles is problematic because of the action of geometric factors related to the size and shape of the particle upon the generation and emission of characteristic X-rays (Goldstein et al., 2003). Various methods have been developed to correct for these geometric effects. An important class of particle corrections is based upon continuously overscanning the particle while collecting the EDS spectrum. This method makes the fundamental assumption that the particle is homogeneous. Although this homogeneity condition is fulfilled for some particle types, it is often found from SEM-BSE images that microscopic particles can consist of aggregates of even finer particles of varying composition. How should we proceed to characterize such aggregates? Overscanning to obtain an "average spectrum" is likely to introduce significant compositional errors, and the localization information is obviously lost. High-speed X-ray spectrum imaging with the SDD offers a powerful tool to elucidate the true compositional nature of a particle. An example of a microscopic particle with a complex microstructure is shown in Figure 7, where the atomic number contrast in an SEM-BSE image reveals a bright inclusion that has a higher average atomic number than the rest of the particle. X-ray maps constructed from a 12-min 160 × 120 pixel XSI show that the particle matrix consists of an alumino-silicate matrix, whereas the inclusion is iron rich. Detailed examination of the additional constituents recognized in the SUM and MAXIMUM PIXEL derived spectra reveal that the particle microstructure is even more complex. For example, the inclusion actually consists of iron and manganese, which are segregated in a very complex fashion that can be best understood through the color overlay. Because the atomic numbers of iron and manganese are separated by only one unit, the BSE compositional contrast between the Fe- and Mn-rich areas of the inclusion is small, about 0.02, which makes it very difficult to discern this complex compositional microstructure by SEM/BSE (Fig. 7a). The XSI maps constructed from peaks recognized in the SUM and MAXIMUM PIXEL derived spectra immediately reveal distinct regions of high iron content and high manganese content, as well as the localization of some elements, such as calcium, whereas others such as potassium are more homogeneous. A single spectrum collected while overscanning this particle would actually be misleading as to the true compositional nature of this particle.

Discussion and Conclusions

The examples presented in the accompanying images suggest just a few of the many possibilities of microstructural characterization that fast XSI mapping with the SDD will make practical. SDD technology has significant advantages over conventional Si(Li)-EDS in terms of output count rate versus input count rate and modest improvements in spectral resolution for a given detector active area. The SDD inevitably has poorer efficiency for high energy photons, above 10 keV in energy, due to the reduced thickness of the SDD, 300 μm, compared to the 3-mm thickness of the Su(Li). However, it is important to realize that this extraordinary SDD X-ray measurement technology is just in its infancy. Commercial SDDs are currently available from several manufacturers, and it is reasonable to expect that further advances in performance will be realized as more development efforts occur from an expanding pool of manufacturers, especially in the area of high-speed digital pulse processing (Newbury, 2005).

Will SDD spectrum image mapping have a role in the conventional electron probe X-ray microanalyzer (EPMA), where mapping is performed with the wavelength dispersive spectrometer (WDS)? WDS mapping has the advantage that the diffraction process shields the X-ray detector from X-ray photons outside the very narrow energy bandpass, about 2–20 eV depending on the diffractor used, of the peak to which the WDS is tuned. Thus when a minor or trace element is to be mapped, the entire count rate capability of the WDS, 100 kHz or higher, can be devoted exclusively to that element of interest because the abundant characteristic X-rays generated from the high-concentration elements of the specimen are prevented from contributing to the detector dead time, providing that the specimen can withstand high beam currents of several hundred nanoamperes or more needed to create the high X-ray production from the trace constituent. Although the SDD will not replace this special advantage of WDS mapping because the SDD is inherently more limited by its spectral resolution in its trace detectability, SDD spectrum image mapping should still be an extremely useful tool for EPMA. SDD mapping can provide a rapid mapping overview of an area of interest for qualitative analysis of the major and minor constituents on a spatially resolved basis. Such information from SDD mapping could prove very useful in deciding on an efficient WDS mapping strategy that could avoid

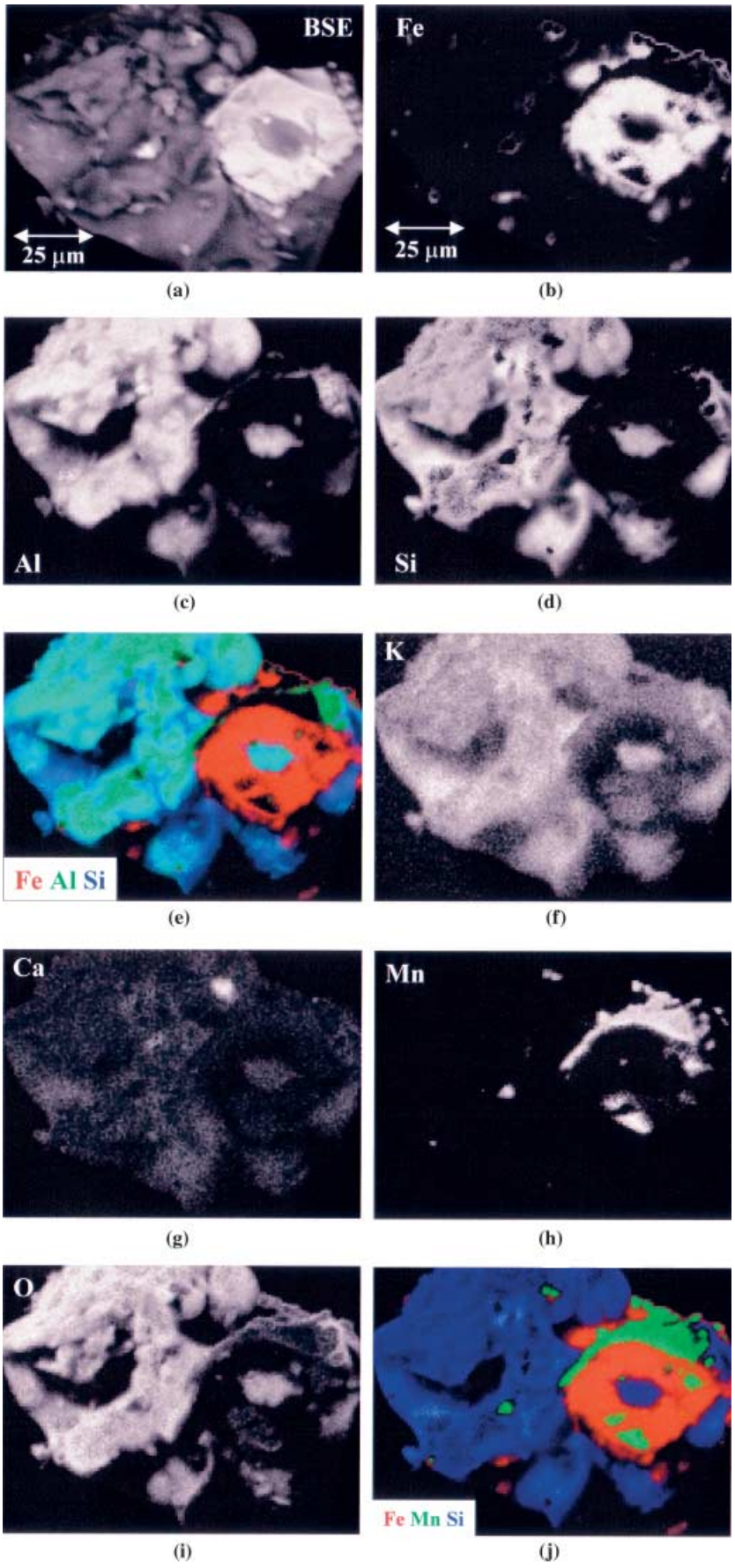

Figure 7. Particle of slag from a coal-fired power plant. **a**: SEM-BSE image. X-ray maps derived from a 12 min 160 × 120 pixel X-ray spectrum image: FeKα (**b**); AlKα (**c**); SiKa (**d**); color overlay, Fe = red, Al = green, Si = blue (**e**); K Kα (**f**); CaKα (**g**); MnKα (**h**); O K (**i**); color overlay, Fe = red, Mn = green, Si = blue (**j**).

the problem of missing elements of interest that might not be detected in an "overscan" spectrum of the area of interest obtained with a conventional Si(Li)-EDS, which is the typical practice.

The convergence of the SDD with (1) high performance Schottky field emission SEMs, which combine high electron source brightness with high total beam current, (2) advanced computer beam control, and (3) spectrum imaging should provide a class of analytical SEMs that can automatically select and map targets following a set of criteria defined by the analyst. Such a system could, for example, automatically tile a target with a series of XSI maps that would completely capture the microscopic compositional variations but over a much larger area than previously practical. Digesting this huge amount of compositional information will be challenging, but such software tools for this problem are under continuous development. The SEM-SDD may finally provide the comprehensive tool to allow the microanalyst to effectively address the "micro to macro" problem. In electron-excited energy dispersive X-ray spectrometry we have an elegant, powerful tool for local analysis with micrometer to nanometer lateral and depth resolution. Yet to solve practical problems, we are frequently challenged to characterize large areas of a specimen, or even many specimens, which constitutes a macroscopic sampling problem. The SEM-SDD with XSI data collection will emerge as one effective approach to solving the micro to macro problem through massive automated data collection and the application of efficient data analysis tools.

Disclaimer

Certain commercial equipment, instruments, or materials are identified in this article to foster understanding. Such identification does not imply recommendation or endorsement by the National Institute of Standards and Technology, nor does it imply that the materials or equipment identified are necessarily the best available for the purpose.

References

Barkan, S., Saveliv, V., Iwanczyk, J., Feng, L., Tull, C., Patt, B., Newbury, D., Small, J. & Zaluzec, N. (2004). A new improved silicon multi-cathode detector (SMCD) for microanalysis and X-ray mapping applications. *Microsc Today* **12**, 36–37.

Bright, D. (1995). MacLispix: A special purpose public domain image analysis program for the Macintosh. *Microbeam Anal* **4**, 151–163.

Bright, D. (2003). Lispix: A new version of MacLispix for the PC is available at http://www.nist.gov/lispix. Source code is available on request.

Cosslett, V.E. & Duncumb, P. (1956). Micro-analysis by a flying spot X-ray method. *Nature* **177**, 1172–1174.

Fitzgerald, R., Keil, K. & Heinrich K. (1968). Solid-state energy-dispersion spectrometer for electron-microprobe X-ray analysis. *Science* **159**, 528–530.

Goldstein, J., Newbury, D., Joy, D., Lyman, C., Echlin, P., Lifshin, E., Sawyer, L. & Michael, J. (2003). *Scanning Electron Microscopy and X-ray Microanalysis*, 3rd ed. New York: Kluwer Academic/Plenum Press.

Gorlen, K., Barden, L., Del Priore, J., Fiori, C., Gibson, C. & Leapman, R. (1984). A computerized analytical electron microscope for elemental imaging. *Rev Sci Instrum* **55**, 912.

Newbury, D. (2005). X-ray spectrometry and spectrum image mapping at output count rates above 100 kHz with a silicon drift detector on a scanning electron microscope. *Scanning* **27**, 227–239.

Newbury, D. & Bright, D. (2005). "Derived Spectra": Software tools for detecting spatial and spectral features in spectrum images. *Scanning* **27**, 15–22.

Small, J. (1976). An elemental and morphological characterization of emissions from the Dickerson and Chalk Point coal-fired power plants. Ph.D. thesis, Department of Environmental Chemistry, University of Maryland.

Struder, L., Fiorini, C., Gatti, E., Hartmann, R., Holl, P., Krause, N., Lechner, P., Longoni, A., Lutz, G., Kemmer, J., Meidinger, N., Popp, M., Soltau, H. & van Zanthier, C. (1998). High resolution nondispersive X-ray spectroscopy with state of the art silicon detectors. *Mikrochim Acta* **15** (Suppl.) 11–19.